RSC Advances

ROYAL SOCIETY OF CHEMISTRY

www.rsc.org/advances

REVISED

New oxovanadium(IV) complexes with pincer ligand obtained *in situ*: experimental and theoretical studies on the structure, spectroscopic properties and antitumour activity.

Anna Adach[a*], Marek Daszkiewicz[b], Małgorzata Tyszka-Czochara[c], Boleslaw Barszcz[d]

[a] *Institute of Chemistry, Jan Kochanowski University, 15G Świętokrzyska Str., 25-406 Kielce, Poland*
[b] *Institute of Low Temperature and Structure Research, Polish Academy of Sciences, 2 Okólna Str., 50-950 Wrocław, Poland*
[c] *Department of Radioligands, Faculty of Pharmacy, Jagiellonian University Medical College, 9 Medyczna Str., 30-688 Kraków, Poland*
[d] *Institute of Molecular Physics, Polish Academy of Sciences, 17 Smoluchowskiego Str., 60-179 Poznań, Poland*

Abstract

Experimental and theoretical studies on the structure and spectroscopic properties of two complexes: $[VOL^1(NCS)_2]$ (**1**) and $[VOL^1(NCS)_2]\cdot C_6H_5CH_3$ (**2**) where L^1-bis(3,5-dimethylpyrazol-1-ylmethyl)amine have been reported.

The products, isolated in one-pot synthesis, contain multipodal pincer ligand L^1 obtained *in situ* from the system containing 1-hydroxymethyl-3,5-dimethylpyrazole (L) as one of the substrates. The crystal structure, electronic (UV-VIS) and infrared (IR) spectra of the complexes have been analyzed. The combined use of experiments and computations allowed a firm assignment of the majority of the observed electronic and vibrational transitions. Theoretical (DFT) calculations have been carried out at the B3LYP/LanL2DZ level to investigate the geometry of **1** and **2**. They were found to be in a good agreement with the experimental results. Additionally biological activity of complex **2** was investigated. The complex **2** exhibited anti-proliferative activity towards panel of human cancer cells (*hepatocellular carcinoma* Hep G2, *lung carcinoma* A549*, colorectal adenocarcinomas* SW 480 and SW 620). The anti-proliferative potency of complex **2** and its higher selectivity towards cancer cells than those of the vanadium salt tested, makes it an interesting candidate for further investigation of its anti-cancer properties.

* Corresponding author, anna.adach@ujk.edu.pl (Anna Adach)

Introduction

Vanadium compounds present wealthy and fascinating chemistry and very interesting biochemical and pharmacological properties. Vanadium is an essential nutritional element but its functions are not fully known and thus ambiguous.[1-2] On the one hand, it is known that vanadium displays relevant biological actions such as insulin-mimicking.[3-4] On the other hand, the toxic effects of vanadium compounds are well documented.[1] Therefore anti-diabetic properties of vanadium complexes are extensively studied [4] and anti-tumour effects of vanadium derivatives are widely investigated.[5].Vanadyl inorganic compounds such as vanadyl sulphate were used as effective therapeutic agents, but unfortunately, some toxic effects were found.[6] It was found that complexation by organic ligands may improve vanadium efficacy and decrease toxic side effects. Vanadyl complexes with *N*-donor ligands such as a pyrazole derivatives have shown very interesting biochemical and pharmacological properties such as insulin-mimetic properties [5], as well as antiparasitic [3d] and antitumour ones.[7]

Given that pyrazole derivatives are widely used in medical treatment, there is an evident connection between chemical structures of compounds from pyrazole family and their pharmacological activity.[8] Moreover, many pyrazolyl complexes have been prepared and probed for therapeutic actions across a spectrum of diseases and anticancer properties comparable with *cis*-dichlorodiamineplatinium(II) (cisplatin).[9] As pyrazole derivatives have found various successful applications in pharmacology, the complexes of pyrazole derivatives and metal ions have recently received considerable attention.[7-9]

In our systematic studies on the oxidation of implant metals in the presence of biologically important compounds, we have explored the systems containing 1-hydroxymethyl-3,5-dimethylpyrazole (L) as one of the substrates. We have found synthetic methods of two kinds of multipodal and multidentate *N*-ligands such as N,N,N-tris and N,N-bis(pyrazolylmethyl)amines created *in situ* from 1-hydroxymethyl-3,5-dimethylpyrazole (L).[10-15] N-substitued pyrazole derivatives such as N,N-bis(pyrazolylmethyl)amines are pincer ligands and analogues of poly(pyrazolyl)borates, called scorpionates. [16,17]

Our goal was to investigate the system containing zerovalent chromium. We hoped to find complexes created from metallic chromium. Unexpectedly, in contrast to the earlier study with zerovalent cobalt [10-13, 15] and nickel[14] chromium was absent in the composition of the isolated product from the [Cr^0-$VOSO_4$-NH_4SCN-pyrazole derivative (L)] system. Instead of this, we synthesized novel vanadium (IV) complex and its solvate, containing a pincer ligand N,N-bis(3,5-dimethylpyrazol-1-ylmethyl)amine which was created *in situ* in a simple one pot

process. Neither these complexes nor such a simple way of creating them have been reported so far.

X-ray structural characterization and biological activity of these complexes were investigated. Additionally, this paper reports anticancer properties of the products investigated. The results obtained may facilitate future development of vanadium complexes with improved anti-tumour activity.

Experimental

Materials and measurements

All the reagents used were purchased from commercial sources and used without further purification. The experiments were carried out in air. Chromium powder, $VOSO_4 \cdot 5H_2O$ and 3,5-dimethylpyrazole-1-methanol (Aldrich Chemical Company) have been used. Elemental analyses were performed with a Perkin Elmer Elemental Analyzer 2400 CHN.

IR spectra of the investigated compounds dispersed in KBr matrix were recorded with Nicolet 380 FTIR spectrophotometer in the region 4000–400 cm^{-1}. The electronic reflectance spectra (range 50000 -5000 cm^{-1}) were measured on a Cary 500 Scan (Varian) UV-VIS –NIR Spectrophotometer. The absorption spectra were recorded on UV-3600 Spectrophotometer (Shimadzu).

Synthesis

Compounds **1** and **2** were synthesized according to the general procedure.[10-15] The reagents: $VOSO_4 \cdot 5H_2O$, 1-hydroxymethyl-3,5-dimethylpyrazole, NH_4SCN and metallic chromium powder (325 mesh) were used in 1: 2:6:1 molar ratio, respectively. Chromium powder (0.0252 g, 0.5 mmol) was added to 30 mL of a methanolic solution of $VOSO_4 \cdot 5H_2O$ (0.12545 g, 0.5 mmol) and NH_4SCN (0.2286g, 3 mmol). Finally, a methanolic solution (30 mL) of 1-hydroxymethyl-3,5-dimethylpyrazole (0.1265g, 1.0 mmol) was added. After one day, 10 mL of CH_3CN was added. The mixture was heated in a round bottomed flask with a Liebig condenser and stirred magnetically to 50-60 ^oC for 25-30 h. The solution was filtered to remove any undissolved material. The resulting bright green solution was left to slow evaporation of the solvent and blue non-crystalline product appeared after two weeks. To obtain crystals suitable for X-ray measurements and collect a sufficient amount for biological studies, this non-crystalline crude product had to be recrystallized from the mixture of toluene, CH_3CN and CH_2Cl_2 (4:2:1), and under a slow evaporation at room temperature, after

two weeks, blue crystals (**2**) appeared. Additionally, it was possible to isolate a few single crystals of (**1**) which appeared occasionally only in the original solution, before the recrystallization, thus making it impossible to test (**1)** biologically.

Compound (**1**) $C_{14}H_{19}N_7S_2VO$ *Elemental analyses: found* (%): for C, 40.15; H, 4.51; N, 24.02; S,12.63 (%). *Calc.* C, 40.37; H, 4.06; N, 23.56; S,12.24 (%).

Compound (**2**) $C_{21}H_{27}N_7S_2VO$ *Elemental analyses: found* (%): for C, 48.96; H, 5.01; N, 19.69; S, 12.95 (%). *Calc.* C, 49.59; H, 5.35; N, 19.29; S,12.58 (%).

X-ray diffraction

X-ray diffraction data were collected on a KUMA Diffraction KM-4 four-circle single crystal diffractometer equipped with a CCD detector using graphite-monochromatized MoK_α radiation (λ=0.71073 Å). Experiments were carried out at 295 K. The raw data were treated with the CrysAlis Data Reduction Program (version 1.172.33.42) taking into account an absorption correction. The intensities of the reflection were corrected for Lorentz and polarization effects. The crystal structure was solved by direct methods [1] and refined by full-matrix least-squares method using SHELXL-2013 and ShelXle programs [18,19] (Table 1). Non-hydrogen atoms were refined using anisotropic displacement parameters. H-atoms were visible on the Fourier difference maps, but placed by geometry and allowed to refine "riding on" the parent atom.

Quantum chemical calculations

The quantum chemical calculations of **1** and **2** were performed using the Gaussian 03 program.[20] The calculations were carried out for isolated molecules using the density functional theory (DFT) with Becke's three parameter exchange functional combined with the Lee–Yang–Parr correlation functional (B3LYP). The experimental (X-ray) crystallographic data were used as an initial geometry. The LanL2DZ basis set was used for geometry optimizations and calculations of the normal modes frequencies. The normal modes description was made by visual inspection of the individual modes using the GaussView program. The transition energies of **1** and **2** have been calculated by means of a time dependent density functional theory (TD-DFT) method with hybrid B3LYP functional and LanL2DZ basis set using the equilibrium geometries of the investigated species obtained in the normal mode frequencies calculations. The part of the TD-DFT results analysis including

the convolution of the calculated transition energies and oscillator strengths into the spectrum was made with the application of the Gauss Sum program.[21]

Biological studies

Cell culture conditions. Human cell lines were derived from the American Type Cell Culture collection, ATCC (LGC Standards-ATCC (Teddington, Great Britain), ATCC designations were as follows: BJ, normal adherent human skin fibroblasts, CRL-2522; HEP G2, *hepatocellular carcinoma,* HB-8065; A549, lung *carcinoma,* CCL-185; SW 480, Dukes' type B colorectal adenocarcinoma, CCL-228; SW 620, Dukes' type C colorectal adenocarcinoma, CCL-227. The skin fibroblasts BJ and HEP G2 cell lines were maintained as a monolayer cultures in Eagle's Minimum Essential Medium (EMEM) while A549, SW 480 and SW 620 were cultured in Dulbecco's Modified Eagle's Medium (DMEM) (PAA Laboratories GmbH, Austria). All the media were supplemented with 10 % v/v FBS (ATCC) and with antibiotic solution (100 IU/mL penicillin, 0.1 mg/mL streptomycin, Gibco Laboratories, NY, USA, Minerva Biolabs, Berlin, Germany). The cells were kept at 37°C in a humidified atmosphere of 5 % CO_2. The cells used in the experiments were between 15^{th} and 25^{th} passages.

In vitro anti-proliferative assay. The in vitro testing of the substances for antitumour activity in adherent growing cell lines was carried out using MTT assay.[22] MTT, (3-[4,5-dimethylthiazol-2yl]-2,5-diphenyl tetrazolium bromide was purchased from Sigma-Aldrich, Seelze, Germany. Briefly, 100 µL of a suspension of exponentially dividing cells was placed in each well of a 96-well microtiter plate at density $1*10^5$ cells per mL of culture medium and incubated overnight at 37 °C in a humidified atmosphere (5% CO_2). Then the medium in each well was replaced with a new one, also containing the adequate volume of a stock solution of tested compounds or the adequate amounts of dimethylsulfoxide (DMSO) solvent. The cells cultured in the medium and the solvent were positive control (100 % of growth). The range of tested concentrations of compounds was 10mM/L-100nM/L. After 24 hours the medium was removed and MTT formazan generated during incubation was dissolved in DMSO and the absorbance was measured at 570 nm (the reference wavelength was 630 nm) using a microplate reader Infinite M200 Pro, Tecan, Austria. For each sample, the final results were expressed using IC 50, a parameter that indicated anti-proliferative potency of chemicals. IC

50 was the concentration [μM/L] of a tested compound required to achieve half maximal inhibition of cells proliferation. [23]

Results and discussion

Two novel mononuclear complexes $[VOL^1(NCS)_2]$ (**1**) and $[VOL^1(NCS)_2]\cdot C_6H_5CH_3$ (**2**) with N-scorpionate ligand where L^1 - bis-(3,5-dimethylpyrazol-1-ylmethyl)amine, were obtained *in situ* from the system containing vanadyl sulphate ($VOSO_4$), pyrazole derivative, ammonium thiocyanate and metallic chromium. Contrary to our previous work [13-15], the zerovalent metal (powdered chromium) present in the reacting system does not appear in the final product. It seems to play a pure catalytical role.[24]

The ammonium thiocyanate plays a dual role - a source of monodentate ligands NCS^- and an indispensable substrate (NH_4^+ ions) for the one-pot synthesis of secondary amine (Scheme 1) through condensation processes (Mannich reactions) (Scheme 1).[25]

This multipodal, tetradentate organic ligand formed *in situ* can be called an "impaired" scorpionate analogue of poly(pyrazolyl)borate ligands, containing only two, instead of three pyrazole groups.

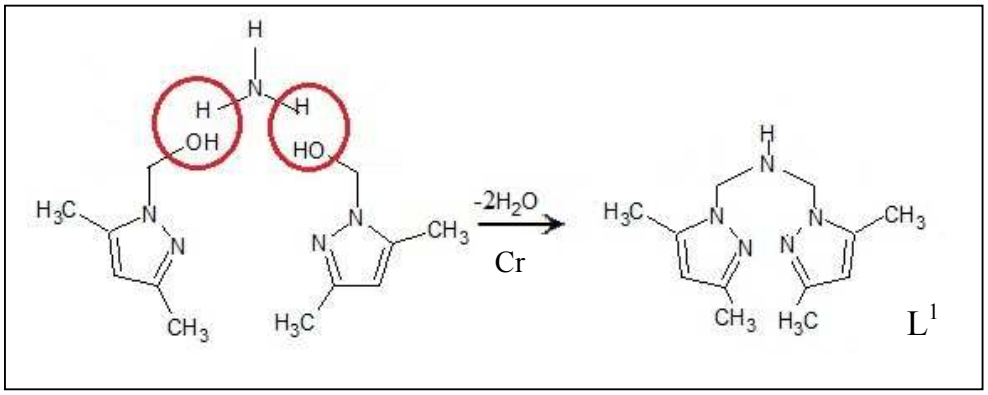

Scheme 1 The route of formation of N,N-bis(3,5-dimethylpyrazol-1-ylmethyl)amine (L^1).

Crystal structures

The studied compounds, $[VOL^1(NCS)_2]$ (**1**) and $[VOL^1(NCS)_2]\cdot C_6H_5CH_3$ (**2**), crystallize in monoclinic crystal system in $P2_1/n$ and $P2_1/m$ space group, respectively (Table 1). In **1**, all the atoms lie in general positions, whereas in **2**, a mirror plane passes through the $[VOL^1(NCS)_2]$ and toluene molecules (Fig 1). This mirror plane is perpendicular to the toluene molecule (Fig. 2b). Complexes **1** and **2** contain a hexacoordinate vanadium(IV) center. The VO^{2+} ion is coordinated by the three nitrogen atoms of the bis-(3,5-dimethylpyrazol-1-ylmethyl)amine

(L^1), forming five-membered chelate rings, and two NCS^- anions in *cis* positions, which balance positive charge of the vanadyl ion. The V=O bond distance is 1.592(2) Å for (**1**) and 1.582 for (**2**) which are typical of oxovanadium complexes.[26,27] The central ion is displaced from the octahedron center towards oxygen atom of the vanadyl ion by 0.38 Å and 0.39 Å in compounds **1** and **2**, respectively. As a result, long V–N1 bond is observed in both compounds (Table 2). The elongation of V-N(1)bond is due to the trans effect of the oxygen, usually observed in the hexacoordinated vanadyl(IV) complexes.[26,27] In both complexes, the V-N bond lengths order is: $V\text{-}N(1)_{(amine)} > V\text{-}N(12)_{(pyrazole)} > V\text{-}N(2)_{(NCS)}$. Such a sequence and a displacement of the central ion have been also observed in our previous studies on cobalt(II) and nickel(II) complexes which contained N,N-bis(3,5-dimethylpyrazol-1-ylmethyl)amine (L^1).[13, 14] However, it is worth noting that in vanadium(IV) complexes, deformation of the coordination sphere is related to the molecular stiffness of the ligand. Vanadium atom in the VO^{2+} ion usually has a deformed coordination sphere of tetragonal pyramidal or bipiramidal geometry.[28, 29] It appears that formation of the $[VOL^1(NCS)_2]$ complex results from the molecular structure matching of the organic ligand and the VO^{2+} ion.

Geometric parameters of intermolecular interactions present in the studied crystals indicate their weak nature (Table 3). Among these, the most important are presented on the Hirshfeld surface (Figure 2ab).[30.31] In $[VOL^1(NCS)_2]$ (**1**), the strongest intermolecular interaction is created by the N–H group and oxygen atom. It appears that this interaction plays an essential role in self-assembly of the molecules because it forms the shortest chain pattern of hydrogen bonds in the structure. The pattern is described by the unitary graph-set descriptor C(4) (Figure 2c).[32,33]

Compound **2** is a solvate, where the toluene molecule is trapped between $[VOL^1(NCS)_2]$ molecules. Comparing a volume of the unit cell for **1** and **2**, it can be simply calculated that one toluene molecule occupies ca. 153.1 $Å^3$. This value is a little bit larger than for α and β-toluene, 143.1 $Å^3$ and 146.1 $Å^3$. [34-38] Thus, it appears that intermolecular interactions where the toluene molecule is engaged are weaker in **2** than in α or β phases of pure toluene. The only significant interaction of toluene molecule in $[VOL^1(NCS)_2]\cdot C_6H_5CH_3$ (**2**) is N–H···π (Figure 2d). Using Malone's criteria for X–H···π interactions, some geometry parameters are calculated $d_{\pi H}$ = 2.43 Å, θ = 82 deg, α = 141 deg, d = 0.33 Å .[39] These values (Table 3) indicate that N–H···π interaction found for the toluene molecule in **2** can be classified as type III. Interestingly, no classical hydrogen bonding patterns are present in the crystal structure of **2**. Instead of these, C17–H17E···π interaction creates a chain of the rings pattern which

propagates along crystallographic direction *b* (Figure 2d). The Malone's parameters $d_{\pi H}$ = 3.21 Å, θ = 27 deg, α = 132 deg, d = 2.86 Å suggest a weak nature of that interaction which is classified as type V .[39]

According to molecular orbital theory , the frontier orbitals and nearby molecular orbitals are the most important factors to stability. The energy values of $\Delta E_{HOMO-LUMO}$ (Table S1) are 3.65 and 3.67 respectively, for complex **1** and **2** which show the order of stability is **2** >**1**. Moreover, the lower total energy value of **2** also suggests higher stability of that structure. In Fig. 3, the calculated frontier molecular orbitals (alpha spin) of **1** (left side) and **2** (right side) are presented. In both cases the, SOMO (single occupied molecular orbital) is located mainly on NCS ligands while the LUMO is centered on the vanadyl moiety.

Fig.1-3 Table 1-3

Infrared spectra

The IR spectra interpretation and bands assignment were made taking into account the results of DFT calculations and literature data. Details of the bands assignment are collected in Table 4 and Figure S1. The calculated stretching frequencies have been found to be in good agreement with the experimental frequencies (Fig. S2).

The IR results are consistent with crystallographic studies of **1** and **2** complexes. The presence of thiocyanato groups in **1** and **2** is visible in the IR (Table 4, Fig. S2 and Fig. S1). The very strong absorption band in 2000-2100 cm^{-1} region was assigned to the stretching vibrations of the NCS^- ions. Generally, thiocyanate ions are versatile ligands that can be bound to metal ions in a variety of ways. Having two different donor atoms, NCS^- ion can act as a monodentate N-bonded or S-bonded ligand as well as a bridging ligand. [40] The appearance of strong split bands in the range of 2040-2080 cm^{-1} ν(CN) confirm the presence of the NCS^- entity in the complexes. [40] The interaction between isotiocyanato ligands S(2)…S(3) is the reason for stretching band ν(CN) splitting, which is visible at 2047 and 2070 cm^{-1} in complex **1** and 2049 and 2072 cm^{-1} in complex **2**. These results correlate well with the X-ray data on monodentate coordination of N-bonded NCS ligand and *cis* position of the isothiocyanate groups with respect to VO^{2+} ion in both studied compounds. [28, 40, 41] The position of strong bands at *ca.* 1550 - 1350 cm^{-1} attributed to the CC and CN stretching vibrations from pyrazole rings (Table 4) confirmed coordination *via* nitrogen atoms of pyrazole rings. Additionally, the characteristic band related to secondary amine (ν CN asymmetric stretching) located at 1245 cm^{-1}, as well as δ_{NH}, provides evidence for the condensation process and

creation of the new organic ligand L^1 being secondary amine. [40,42] In the calculated spectra, the amine CN stretching is located at 1184 cm^{-1} and it is not so distinct as in experimental spectrum. On the other hand, there is a strong band related to the NN stretching and N-CH_2 stretching at 1262 cm^{-1}, which can be attributed to the experimental band at 1245 cm^{-1}. Such a slight discrepancy was observed for other secondary amines and their complexes. [42]

In addition, the compounds exhibit a strong band in the 970–990 cm^{-1} region due to the terminal V=O stretching. [28, 41,43]

The V=O stretching vibrations were observed at 973 and 982 cm^{-1} for **1** and **2**, respectively. On the basis of the IR studies on various oxovanadium(IV) complexes, it is reasonable to conclude that there is an overall trend in the wavenumber for ν(V=O). Vanadyl complexes with coordination number of 6 show lower corresponding stretching vibration (below 995 cm^{-1}) than 5-coordinated. [28, 44] Thus, the IR observations are in line with the crystallographic conclusions, as both the oxovanadium(IV) complexes studied here, have the coordination number of 6 and are similar to those observed for other 6-coordinate V=O complexes.[28,41,44] Moreover, relatively weak agreement between the calculated and experimental IR spectrum in the region of VO stretching suggests that the vanadyl group is involved in some interaction not included in DFT calculations.

The spectrum of **2** (Fig.S1) clearly shows the presence of toluene molecule. The bands at 1114 cm^{-1} and 754 cm^{-1} are in line with the literature data and confirm the presence of toluene molecule in **2.** [45] Moreover, the calculated spectra of (**2**) (see Fig. S2) also show features related to the toluene molecule vibrations at 728 and 776 cm^{-1}, which can be assigned to the experimentally observed bands (see Table 4 for details).

Table 4

Electronic spectra

The theoretical spectra calculated for **1** and **2** (Fig S3) are almost the same, therefore we present in detail experimental data of $[VOL^1(SCN)_2]\cdot C_6H_5CH_3$.

The spectral results for the complex $[VOL^1(SCN)_2]\cdot C_6H_5CH_3$ are characteristic of a pseudo octahedral geometry around the central vanadium(IV) ion [46] and are consistent with vanadyl complexes as predicted by Ballhausen and Gray.[47] The reflectance spectra of $[VOL^1(SCN)_2]\cdot C_6H_5CH_3$ show broad bands in the visible and UV regions (Fig.4).

Generally, a single transition can be expected for the V(IV) ion with $3d^1$ configuration in an octahedral symmetry. However, vanadium(IV) ion most frequently exists as vanadyl VO^{2+} ion in an octahedral environment and the symmetry is lowered due to the tetragonal distortion. [28,29, 46] Therefore, according to the Ballhausen and Gray ligand field model for the one

electron transitions, three d-d bands were expected for 6-coordinated oxovanadium(IV) complexes. [41,47] The solid state visible spectrum of $[VOL^1(SCN)_2]\cdot C_6H_5CH_3$ (**2**) shows the characteristic bands typical of octahedral vanadyl(IV) complexes. [28, 46,47] Of the three expected low-energy ligand field bands, two are easily observed in the 12870-13330cm^{-1} and 16950- 17860 cm^{-1}) ranges and are assigned as $^2B_{2g} \rightarrow {}^2E$, ($d_{xy} \rightarrow d_{xz}$, d_{yz}) (ν_1), and $^2B_{2g} \rightarrow {}^2B_{1g}$ ($d_{xy} \rightarrow d_x^2 - d_y^2$) ($\nu_2$), transitions. The third one (ν_3) assigned to $^2B_2 \rightarrow {}^2A_1$ ($d_{xy} \rightarrow d_z^2$) transition is not clearly visible in reflectance spectra because it is covered by charge transfer absorptions (overlaping high energy bands in the 25000-48500 cm^{-1} range). On dissolution in methanol, relatively distinct well-separated bands were obtained (Fig. 4 insert) (Table 5). The value of extinction coefficients can be assigned to the nature of electronic transitions [46, 47].

The symmetry of the oxovanadium (IV) complex is confirmed by calculated tetragonal crystal field parameters D_q, D_s and D_t (Table 5) [28] which are typical of a vanadium(IV) ion existing as a VO^{2+} group in octahedral coordination with tetragonal compression [47] (see crystallographic section). These spectral data are consistent with those predicted for six-coordinate tetragonal oxovanadium(IV) complexes of (C_{4v}) symmetry.[28, 46, 48, 49] This deformation may be ascribed to $[VON_3N_2']$ chromophore of vanadium(IV) which is a consequence of perturbation by axial V=O group and interactions with different nitrogen atoms of two types of ligands (L^1 and NCS^-). These results are consistent with crystallographic data of **2**, which shows that the V=O bond length in **2** is somewhat shorter (1.582 Å) than might be expected of six-coordinate V=O bond (1.62 Å) **-** in contrast to typical vanadyl complexes VOL_5 ($[VO(H_2O)_5]^{2+}$ and $[VO(NCS)_5]^{3-}$). [46]

Finally, for a more quantitative description of the electronic absorption spectrum, the type of electronic transitions was investigated by DFT calculation (Table 6 Fig. S2) Most of the transitions with a significant oscillator strength fall into the region above 20000 cm^{-1}. Almost all of them involve ligand and vanadyl orbitals during the transition ($L^1 \rightarrow$ VO and $L^{NCS} \rightarrow$V(IV)) . A detailed description can be found in Table 6 (this table is limited to transitions with oscillator strength>0.02).

Fig. 4 Table 5-6

Biological studies

The inhibitory potency of compounds was characterized using MTT assay. The ability of $[VOL^1(SCN)_2]C_6H_5CH_3$ to inhibit the cell growth and metabolism was evaluated according to the reference salts, which were used as substrates: vanadyl(IV) sulfate ($VOSO_4\cdot 5H_2O$) and ammonium thiocyanate (NH_4NCS). A panel of human cancer cells (*hepatocellular carcinoma* Hep G2, *lung carcinoma* A549*, colorectal adenocarcinomas* SW 480 and SW 620*)* was

chosen for the anti-proliferative assay. To determine the selectivity of compounds, the influence on tumour cells was compared to the effect measured in normal human fibroblasts (BJ) and hamster ovary cells (CHO-K1).

The anti-proliferative potency of $[VOL^1(SCN)_2]\cdot C_6H_5CH_3$ and its substrates is presented in Table 7.

Anti-proliferative activity against tumour cells

Given that coordination processes with organic ligands may change biological activity of metals ions, we compared a cytotoxicity profile of isolated $[VOL^1(SCN)_2]\cdot C_6H_5CH_3$ complex and $VOSO_4$ and NH_4SCN used as substrates. Biological results show that IC_{50} values for $[VOL^1(SCN)_2]C_6H_5CH_3$ in tumour cells are clearly lower, compared with the inhibitory effect measured for vanadyl(IV) sulphate used as a substrate (Table **7**). In general, complex **2** after 24h of incubation with cells exhibits anti-proliferative activity towards cancer cell lines, whereas vanadyl(IV) sulfate reveals minor cytotoxicity towards tumour cells. The ammonium thiocyanate is inactive in all the cell lines tested, both tumour and normal ones.

The results obtained show that $[VOL^1(SCN)_2]\cdot C_6H_5CH_3$ exerts comparable anti-proliferative potential towards distant-originated human carcinomas such as Hep G2, A549 and SW 480. Notably $[VOL^1(SCN)_2]\cdot C_6H_5CH_3$ is cytotoxic, both towards SW480 and SW 620 cells, the latter being at a more advanced stage of tumourigenesis than the former. Moreover, 2-fold differences in the anti-proliferative potency were found between both tested *colorectal adenocarcinomas,* SW 480 and SW 620, with corresponding values IC_{50} 323,6±8,8 μM and IC_{50} 635,9±9,6 μM, respectively.

The observed alterations of cells response according to different degree of invasion of colorectal cancer may imply that the mechanism of $[VOL^1(SCN)_2]\cdot C_6H_5CH_3$ action could differ in specificity towards metastatic cells. Therefore, in order to elucidate the mechanism of these phenomena, the study will be continued.

Anti-proliferative activity against normal cells

Investigated compounds were tested also towards non-tumour human fibroblasts (BJ) and hamster ovary cells (CHO-K1) (Table 7). Considering the effect of the tested compounds towards normal cells, both vanadium derivatives: complex $[VOL^1(SCN)_2]\cdot C_6H_5CH_3$ and vanadyl(IV) sulfate, exert an anti-proliferative effect on human fibroblasts. The effect of complex **2** is more pronounced compared with vanadium salt (IC_{50} 189,6±10,9 μM vs. IC_{50} 245,1±12,9 μM). It is worth noting that while vanadyl(IV) sulfate is cytotoxic only toward normal fibroblasts, complex **2** inhibits the growth of cancer cells as well (Table 7), which may denote that complex **2** expresses higher specificity towards tumour cells than vanadyl(IV)

sulfate. This is a positive finding, regarding well published anti-neoplastic performance of the latter. [51, 52, 53] In the present experiments, normal hamster ovary cells (CHO-K1) are the most susceptible ones to the compounds tested.

The high anti-proliferative potency towards non-tumour cell may be regarded as an unfavorable effect, but it should be emphasized that also platinum(II) compounds, used in 50% of all cancer therapies, are known to cause adverse systemic effects in patients and are cytotoxic towards all cells, not only cancer ones. When comparing IC_{50} values for cisplatin (cis-$[Pt(NH_3)_2(Cl)_2]$) towards cancer cell line and its normal counterpart, cisplatin may appear more cytotoxic towards normal cells than tumours, as was shown for *lung carcinoma* A549 and normal lung fibroblasts MRC-5 cell line. [54]

Vanadium salts, including vanadyl(IV) sulfate, have been suspected to exert toxic effects on human liver. [50] It was demonstrated that organic vanadium compounds in general are safer than inorganic vanadium salts, but published data are ambivalent. Therefore, taking into consideration the potent anti-tumour effect of vanadium compounds, search for new complexes that possess low toxicity combined with high efficiency is highly required.

Summing up, the anti-proliferative action of newly synthesized $[VOL^1(SCN)_2]\cdot C_6H_5CH_3$ complex has been found not to depend upon the performance of complex substrates (including VO^{2+} and NCS^- groups), which separately were non-toxic towards cancer cells. The potent anti-proliferative activity of complex **2** and higher selectivity towards cancer cells than vanadium salts make it an interesting candidate for further investigation of anti-cancer properties.

Table 7

Summary and Conclusions

Complexes **1** and **2** were obtained successfully from one-pot synthesis. Both complexes contain vanadyl(IV) ions coordinated to NCS^- ions and multipodal pincer ligand (L^1). This ligand (L^1) is the secondary amine obtained *in situ* from the system containing 1-hydroxymethyl-3,5-dimethylpyrazole (L). Compounds **1** and **2** are characterized by elemental analysis, spectroscopic studies and single-crystal X-ray diffraction.

The spectroscopic analysis is in agreement with the crystallographic data. The results show that the isolated compounds are mononuclear, sixcoordinate vanadium(IV) species with distorted tetragonal symmetry. The VO^{2+} ion binds three nitrogen atoms of the bis(1-(3,5-dimethylpyrazolylmethyl)amine and two NCS^- anions which balance positive charge of the vanadyl ion.

The symmetry of the oxovanadium(IV) complex is confirmed by calculated tetragonal crystal field parameters D_q D_s, and D_t.

Complex $[VOL^1(NCS)_2]\cdot C_6H_5CH_3$ exhibited anti-proliferative activity towards a panel of human cancer cells, with respect to a tissue- origin and a degree of invasion.

The comparison of cytotoxic profile of substrates, vanadium salt ($VOSO_4\cdot 5H_2O$) and ammonium thiocyanate (NH_4NCS), with complex **2** revealed that all the substrates exhibit low ($VOSO_4\cdot 5H_2O$) or even no (NH_4NCS) anti-proliferative activity towards tumour cells. The anti-proliferative potency of complex **2** and higher selectivity towards cancer cells than tested vanadium salt makes it an interesting candidate for further investigation of anti-cancer properties.

Supplementary materials

CCDC-1407700 (**1**) and CCDC-1407701 (**2**) contain the supplementary crystallographic data for this paper. These data can be obtained free of charge via www.ccdc.cam.ac.uk/conts/retrieving.html (or from the Cambridge Crystallographic Data Centre, 12 Union Road, Cambridge CB21EZ, UK: fax: +44 1223 336033; or deposit@ccdc.cam.uk).

Acknowledgments

The authors are thankful to Ms K. Gągrowska and Ms K. Woźnica for help in the synthesis of the complexes and Ms D. Grabka for recording absorption spectra in Structural Laboratory of the Jan Kochanowski University in Kielce.

References

1 (a) D. C. Crans, J. J. Smee, E. Gaidamauskas, L. Yang, *Chem. Rev*., 2004, **104**, 849; (b) D. Rehder, *Coord. Chem. Rev*. 1999, **182,** 297-322; (c) J. L. Domingo, *Reprod. Toxicol*. 1996, **10**, 175-182.

2 M. W. Makinen, M. Salehitazangi; *Coord. Chem. Rev*., 2014, **279**, 1–22.

3 (a) S. Takeshita, I. Kawamura, T. Yasuno, C. Kimura, T. Yamamoto, J. Seki, A. Tamura, H. Sakurai, T. Goto, *J. Inorg. Biochem*., 2001, **85**, 179, (b) J. Benítez, L. Guggeri, I. Tomaz, J. C. Pessoa, V. Moreno, J. Lorenzo, F. X. Avilés, B. Garat, D. Gambino, *J. Inorg. Biochem*., 2009, **103**, 1386, (c) J. Benítez, L. Guggeri, I. Tomaz, G. Arrambide, M. Navarro, J. C. Pessoa, B. Garat, D. Gambino, *J. Inorg. Biochem*.,

2009, **103**,609, (d) J. Benítez, L. Becco, I. Correia, S. Milena Leal, H. Guiset, J. Costa Pessoa, J. Lorenzo, F. Aviles, P. Escobar, V. Moreno, B. Garat, D. Gambino, *J. Inorg. Biochem*., 2011, **105**, 303.

4 Y. Shechter, I. Goldwaser, M. Mironchik, M. Fridkin, D. Gefel, *Coord. Chem. Rev*., 2003, **23**, 7 3-11.

5 (a) A. M. Evangelou, *Crit. Rev. Oncol. Hematol*., 2002, **42**, 249–265, (b) R. S. Ray, B. Ghosh, A. Rana, M. Chatterjee, *Int. J. Cancer*, 2007, **120**, 13–23.

6 H. J. Thompson, D. N Chasteen, L Neeker. *Carcinogenesis*, 1984, **5**, 849–851.

7 S. Holmes C. J. Carrano, *Inorg. Chem*., 1991, **30**, 1231-1235.

8 T Harit, F. Malek, B. El. Bali, A. Khan, K. Dalvandi, B. Marasini, S. Noreen, R. Malik, S. Khan, M. Choudhary, *Med. Chem. Res*., 2012, **21**, 2772-2778.

9 (a) F. K. Keter, S. Kanyanda, J. Darkwa, D. J. G. Rees, M. Meyer, *Cancer Chemother. Pharmacol*., 2008, **63**, 127–138;(b) S. Komeda M, Lutz, A.L. Spek, M. Chikuma, J. Reedijk , *Inorg. Chem*., 2000, **39**, 4230–4236; (c) C. Pettinari, F. Caruso, N. Zaffaroni, R. Villa, F. Marchetti, R. Pettinari, C. Phillips, J. Tanski, M. Rossi, *J. Inorg. Biochem*., 2006, **100**, 58–69.

10 A. Adach, M. Daszkiewicz, B. Barszcz, M. Cieślak-Golonka, G. Maciejewska, *Inorg. Chem. Comm*., 2010, **13**, 361–364.

11 A. Adach, M. Daszkiewicz, B. Barszcz, *Struct. Chem.*, 2010, **21**, 331–336.

12 A. Adach, M. Daszkiewicz, M. Cieślak-Golonka, *Polyhedron*, 2012, **47**, 104–111.

13 A. Adach, M. Daszkiewicz, M. Duczmal, Z. Staszak, *Inorg. Chem. Comm*., 2013, **35**, 22–26.

14 A. Adach, M. Daszkiewicz, , M. Cieślak-Golonka, T. Misiaszek, D. Grabka, *Polyhedron*, 2014, **78**, 31–39.

15 A. Adach, M. Daszkiewicz, B. Barszcz, *Polyhedron*, 2015, **95**, 60–68.

16 (a) S. Trofimenko, Chem. Rev., 1993, **93**, 943-980; (b) S. Trofimenko, *Polyhedron*, 2004, **32**, 197-203; (c) C. Pettrenari, N. Masciocchi, *J. Organomet. Chem*., 2005, **690**, 1871-1877

17 E. Kime-Hunt, K. Spartalian, M. DeRusha, C. M. Nunn, C. J. Carrano , *Inorg. Chem*., 1989, **28**, 4392-4399.

18 G. M. Sheldrick, *Acta Crystallogr. Sec. A*, 2008, A**64**, 112–122.

19 C. B. Hübschle, G. M. Sheldrick, B. Dittrich, *J. Appl. Cryst*., 2011, **44**,1281–1284.

20 Gaussian 03, Revision D.01. M.J. Frisch, G.W. Trucks, H.B. Schlegel, G.E. Scuseria, M.A. Robb, J.R. Cheeseman, J.A. Montgomery, Jr., T. Vreven, K.N. Kudin, J.C.

Burant, J.M. Millam, S.S. Iyengar, J. Tomasi, V. Barone, B. Mennucci, M. Cossi, G. Scalmani, N. Rega, G.A. Petersson, H. Nakatsuji, M. Hada, M. Ehara, K. Toyota, R. Fukuda, J. Hasegawa, M. Ishida, T. Nakajima, Y. Honda, O. Kitao, H. Nakai, M. Klene, X. Li, J.E. Knox, H.P. Hratchian, J.B. Cross, C. Adamo, J. Jaramillo, R. Gomperts, R.E. Stratmann, O. Yazyev, A.J. Austin, R. Cammi, C. Pomelli, J.W. Ochterski, P.Y. Ayala, K. Morokuma, G.A. Voth, P. Salvador, J.J. Dannenberg, V.G. Zakrzewski, S. Dapprich, A.D. Daniels, M.C. Strain, O. Farkas, D.K. Malick, A.D. Rabuck, K. Raghavachari, J.B. Foresman, J.V. Ortiz, Q. Cui, A.G. Baboul, S. Clifford, J. Cioslowski, B.B. Stefanov, G. Liu, A. Liashenko, P. Piskorz, I. Komaromi, R.L. Martin, D.J. Fox, T. Keith, M.A. Al-Laham, C.Y. Peng, A. Nanayakkara, M. Challacombe, P.M.W. Gill, B. Johnson, W. Chen, M.W. Wong, C. Gonzalez, J.A. Pople., *Gaussian, Inc*., Wallingford CT, 2004.

21 N. M. O,,Boyle, A. L. Tenderholt, K. M. Langner, *J. Comb. Chem*., 2008, **29**, 839–845.

22 (a) M. Tyszka-Czochara , P. Paśko, W. Reczyński, M. Szlósarczyk, B. Bystrowska, W. Opoka, *Biol Trace Elem Res*., 2014, **160**, 123–131; (b) P. Pasko, K. Bukowska-Strakova, J. Gdula-Argasinska, M. Tyszka-Czochara *J. Med. Food*., 2013, **16**, 749-759.

23 A. Legin, M. Jakupec, N. Bokach, M. Tyan, V. Kukushkin, B. Keppler, *J. Inorg. Biochem*., 2014, **133**, 33-39.

24 a) J. H. Rigby, K. M. Short, H.S. Ateeq, J. A. Henshilwood, *J. Org. Chem*., 1992, **57** 5290-5291; (b) F. Blank, Ch. Janiak, *Coord. Chem. Rev*., 2009, **253** 8827-861; (c) J. H. Rigby, M. A. Kondratenko, Ch. Fiedler, *Org. Lett*., 2000, **2**, 3917-3919; (c) J. H. Rigby, M. A. Kondratenko, C. Fiedler, *Org. Lett*., 2000, **2**, 3917-3919.

25 S. G. Subramaniapillai, *J. Chem. Sci*., 2013, **125**, 467–482.

26 Y. Dong, R. K. Narla, E. Sudbeck, F. M. Uckun, *J. Inorg. Biochem*., 2000, **78**, 321–330.

27 B. J. Hamstra, A. L. P. Houseman, G. J. Colpas, J. W. Kampf, R. LoBrutto, W. D. Frasch, V. L. Pecoraro, *Inorg. Chem*., 1997, **36**, 4866–4874.

28 E. J. Baran, *J. Coord. Chem*., 2001, **51**, 215-238.

29 D. C. Crans, M. L. Tarlton , C. C. McLauchlan, Eur. *J. Inorg. Chem*. 2014, 4450–4468.

30 F. L. Hirshfeld, *Theor. Chim. Acta*, 1977, **44**, 129.

31 J. J. McKinnon, D. Jayatilaka, M. A. Spackman, *Chem. Commun*., 2007, 3814-3816.

32 M.C. Etter, J. C. MacDonald, J. Bernstein, *Acta Crystallogr., Sect. B: Struct. Sci*. 1990, **46**, 256-262.

33 M. Daszkiewicz, *Struct. Chem*., 2012, **23**, 307-313.

34 F. H. Allen, *Acta Cryst. B*, 2002, **58**, 380–388.

35 I. J. Bruno, J. C. Cole, P. R. Edgington, M. Kessler, C. F. Macrae, P. McCabe, J. Pearson, R. Taylor, *Acta Cryst. B,* 2002, **58**, 389–397.

36 M. Anderson, L. Bosio, J. Bruneaux-Poulle, R. Fourme, *J. Chim. Phys. Phys. - Chim. Biol.* 1977, **74**, 68.

37 S. K. Nayak, R. Sathishkumar, T. N. G. Row, *Cryst.Eng.Comm*., 2010, **12**, 3112.

38 D. Andre, R. Fourme, J. Bruneaux-Poulle, L. Bosio, *J. Mol. Struc*., 1982, **81**, 253-259.

39 J. F. Malone, C. M. Murray, M. H. Charlton, R. Docherty, A. J. Lavery, *J. Chem. Soc., Faraday Trans.*, 1997, **93**, 3429-3436

40 K. Nakamoto, *Infrared and Raman Spectra of Inorganic and Coordination Compounds,* fourth ed., John Wiley, New York, 2009.

41 J. Selbin, *Chem. Rev*., 1965, **65**, 153-175.

42 (a) R. A. Heacock, L. Marion, *Can. J. Chem*,. 1956, **34**, 1782-1795**;** (b) G. Esquius, J. Ponds, R. Yáñez, J. Ros, *J. Organomet. Chem*., 2001, 619, 14–23.

43 M. R. P. Kurup, E. B. Seena**,** M. Kuriakose**,** *Struct. Chem*., 2010, **21**, 599–605.

44 K. Kawabe, M. Tadokoro , K. Hirotsu , N.Yanagihara, Y. Kojima, *Inorg. Chim. Acta*, 2000, **305**, 172-183.

45 J. K. Wilmshurst, H. J. Bernstein, *Can. J. Chem*., 1957, **35**, 911-925.

46 B.P. Lever *Inorganic Electronic Spectroscopy*, second ed. Elsevier, Amsterdam, New York, Tokyo, 1984.

47 C. J. Ballhausen, H. B. Gray, *Inorg. Chem.*, 1962, **1,** 111-122.

48 J. R. Winkler, H. B. Gray, *Struct. Bond*, 2012, **142**, 17–28.

49 M. Kosugi, S. Hikichi, M. Akita, Y. Moro-oka, *Inorg. Chem*., 1999, **38**, 2567-2578.

50 A. K. Srivastava, *Mol. Cell. Biochem*., 2000, **206**, 177–182.

51 (a) H. J. Thompson, D. N. Chasteen, L. Neeker, *Carcinogenesis* 1984, **5**, 849–851; (b) B. Duff, V. R. Thangella, B. S. Creaven, M. Walsh, D. A Egan, *Eur. J. Pharmacol*., 2012, **689**, 45-55; (c) L. A. Nolte D. H. Han, P. A. Hansen, K. A Hucker, J. O. Holloszy, *Diabetes*, 2003, **52**, 1918-1925.

52 A. Bishayee, A. Waghray, M. A. Patel, M. Chatterjee, *Cancer Lett*., 2010, **294**, 1–12.

53 (a) E. Turrini, L. Ferruzzi, C. Fimognari, *Expert Opin. Drug Metab. Toxicol.*, 2014, **10**, 1677-1690. (b) A. Bishayee, A. Waghray, M. A. Patel, M Chatterjee, *Cancer Lett.*, 2010, **294**, 1–12.

54 S. Dhar, S. J. Lippard, *Proc. Natl. Acad. Sci .U S A.*, 2009, **106**, 22199-22204.

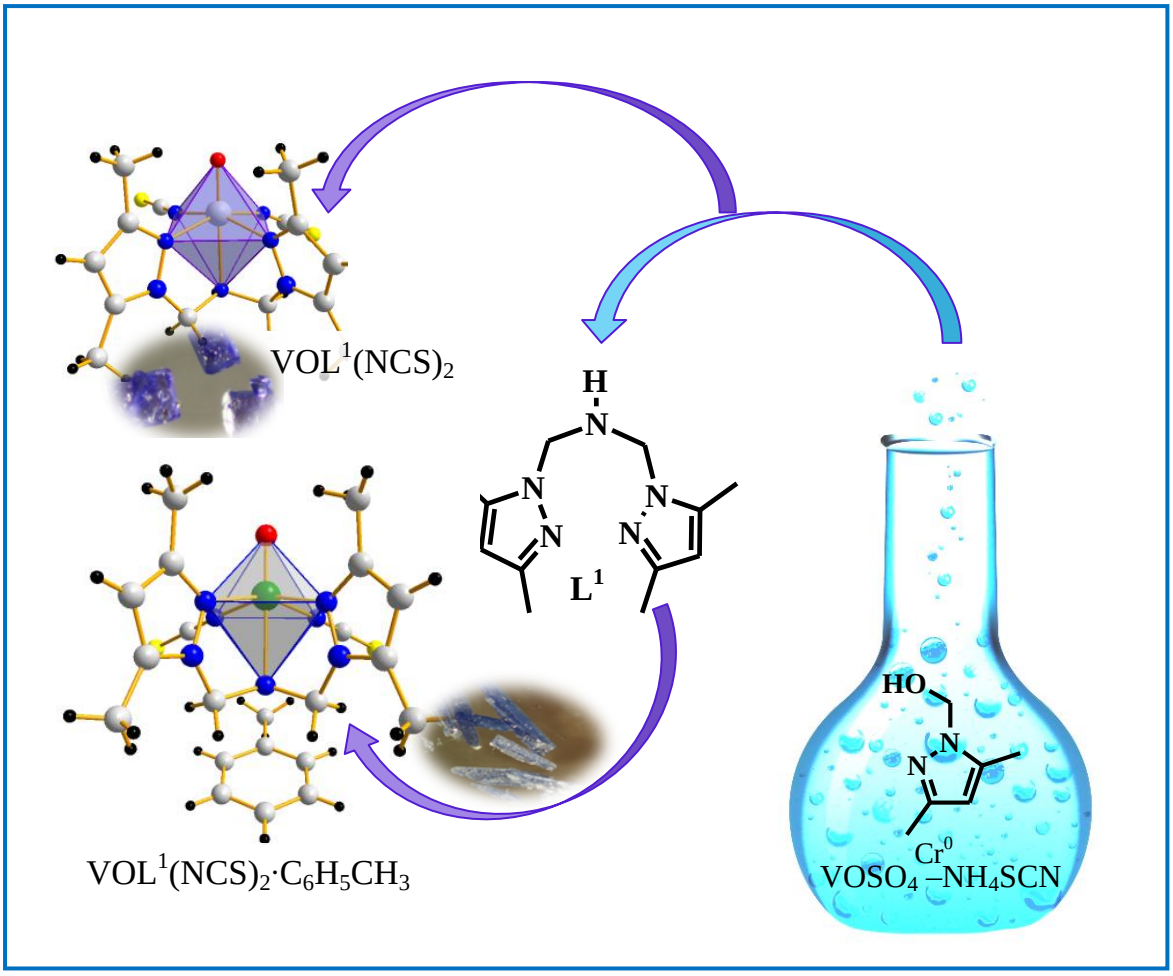

Abstract

Experimental and theoretical studies on the structure and spectroscopic properties of two complexes: $[VOL^1(NCS)_2]$ (**1**) and $[VOL^1(NCS)_2]\cdot C_6H_5CH_3$ (**2**) where L^1-bis(3,5-dimethylpyrazol-1-ylmethyl)amine have been reported.

The products, isolated in one-pot synthesis, contain multipodal princer ligand L^1 obtained *in situ* from the system containing 1-hydroxymethyl-3,5-dimethylpyrazole (L) as one of the substrates. The crystal structure, electronic (UV-VIS) and infrared (IR) spectra of the complexes have been analyzed. The combined use of experiments and computations allowed a firm assignment of the majority of the observed electronic and vibrational transitions. Theoretical (DFT) calculations have been carried out at the B3LYP/LanL2DZ level to investigate the geometry of **1** and **2**. They were found to be in a good agreement with the experimental results. Additionally biological activity of complex **2** was investigated. The complex **2** exhibited anti-proliferative activity towards panel of human cancer cells (*hepatocellular carcinoma* Hep G2, *lung carcinoma* A549*, colorectal adenocarcinomas* SW 480 and SW 620). The anti-proliferative potency of complex 2 and its higher selectivity towards cancer cells than those of the vanadium salt tested, makes it an interesting candidate for further investigation of its anti-cancer properties.

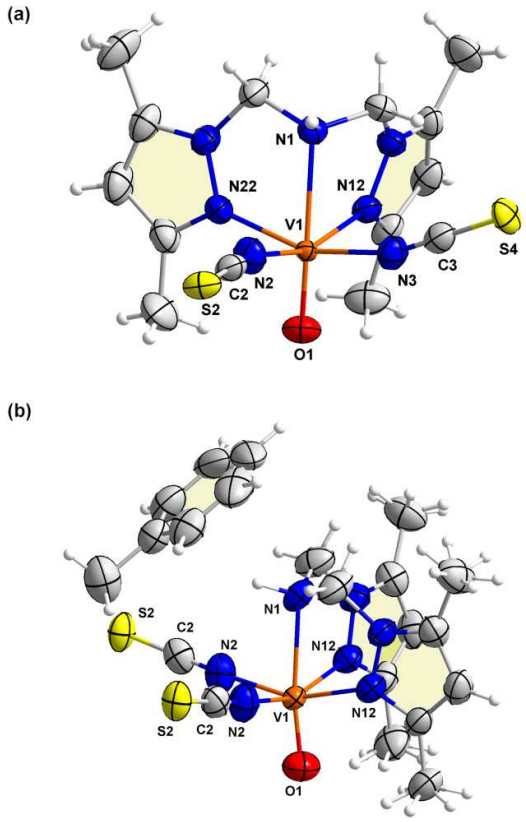

Fig. 1.(a) Molecular structure of [VOL^{1}(NCS)$_2$] (**1**) and (b) [VOL^{1}(NCS)$_2$]·Toluene (**2**).

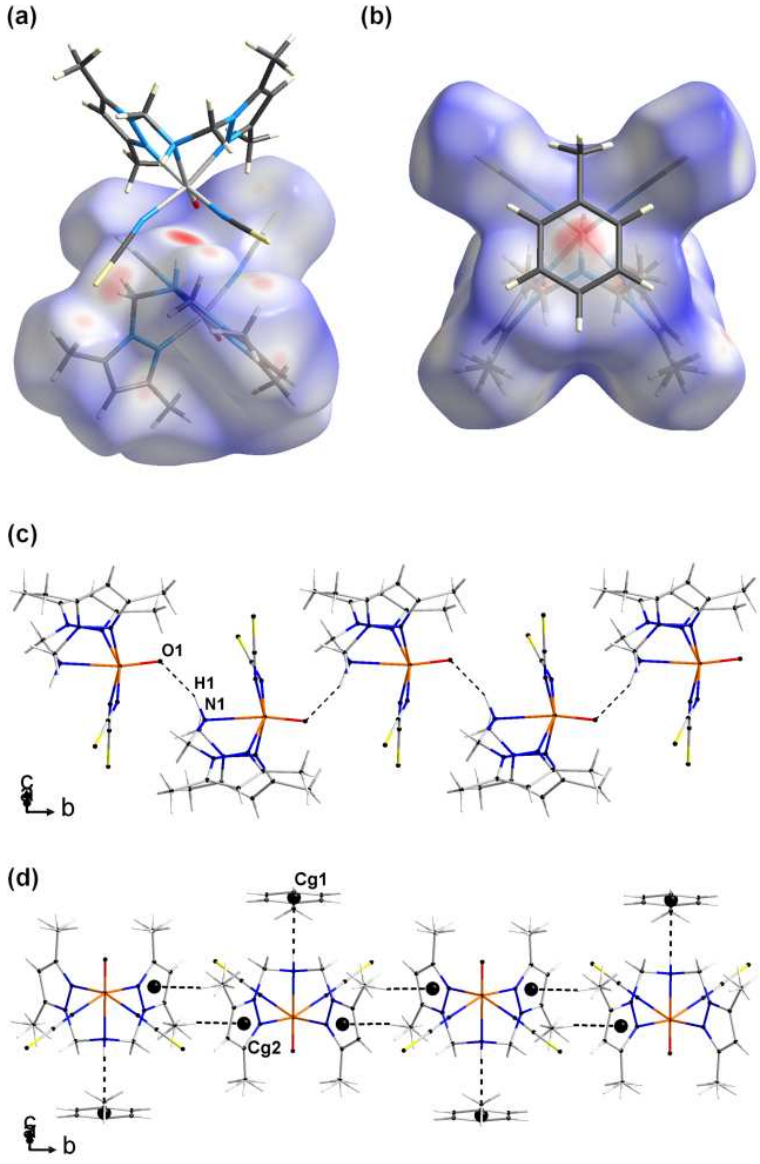

Fig.2. Normalized Hirshfeld surface around the [VOL^1(NCS)$_2$] molecules (a) in **1** and (b) in **2**. Chain patterns created (c) by hydrogen bonds in **1** and (d) by C–H$\cdots\pi$ interactions in **2**.

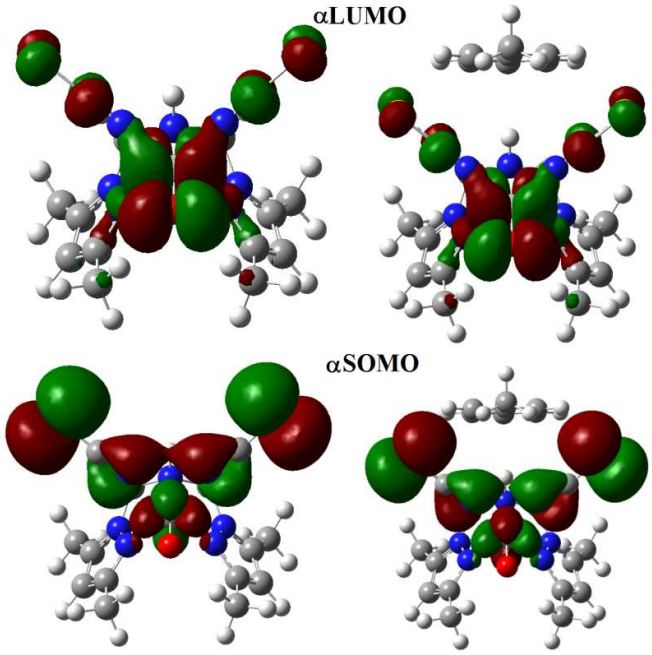

Fig. 3 The contour plots of the frontier molecular orbitals of **1** (left) and **2** (right). Theory level: B3LYP/LanL2DZ

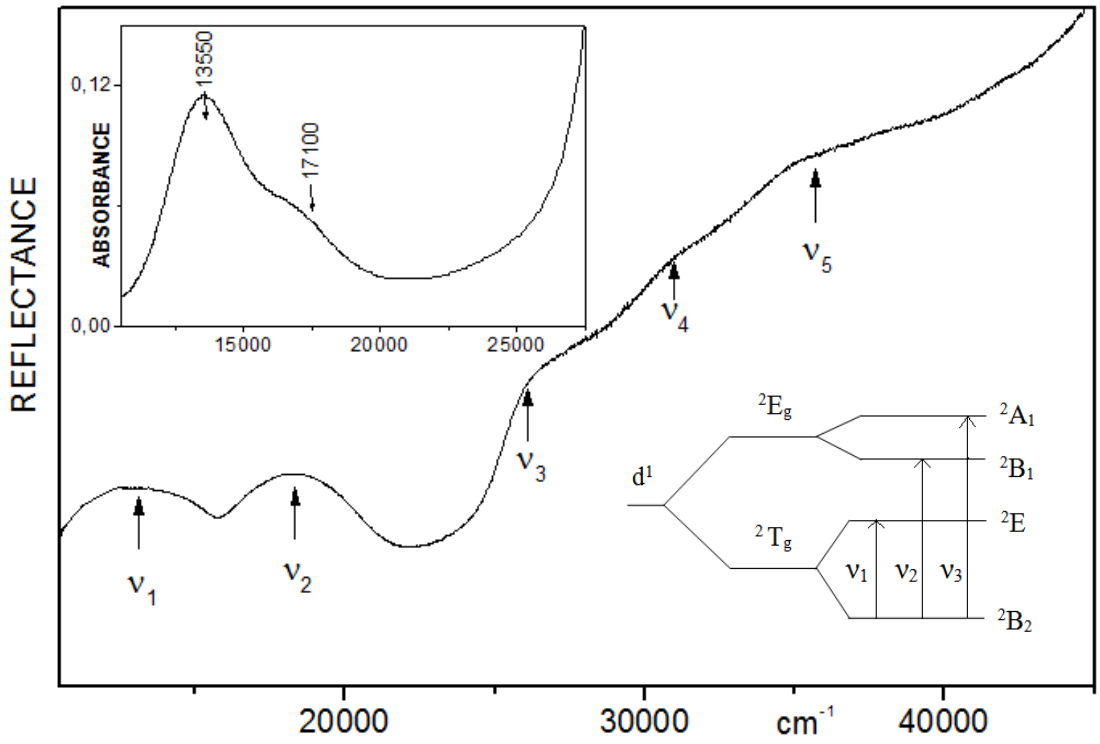

Fig. 4 Diffuse reflectance spectra of $[VOL^{1}(SCN)_2]\cdot C_6H_5CH_3$ (2) and (insert) absorption spectrum of (2) in methanol ($2\cdot10^{-3}$ M, $\varepsilon/M^{-1}cm^{-1}$)

Table 1 Crystal data and structure refinement for **1** and **2**.

	1	**2**
Chemical formula	$C_{14}H_{19}N_7OS_2V$	$C_{14}H_{19}N_7OS_2V{\bullet}C_7H_8$
M_r	416.42	508.55
Crystal system, space group	Monoclinic, $P2_1/n$	Monoclinic, $P2_1/m$
a, b, c (Å)	8.8544(4), 11.2802(4), 19.5722(8)	7.7159(7), 16.2503(12), 10.3876(8)
b (°)	100.708(4)	103.466(9)
V (Å^3), Z	1920.82(14), 4	1266.65(18), 2
m (mm^{-1})	0.75	0.58
Crystal size (mm)	0.25 × 0.22 × 0.13	0.43 × 0.24 × 0.07
T_{min}, T_{max}	0.84, 0.93	0.85, 0.97
No. of measured, independent and observed [$I > 2s(I)$] reflections	22463, 3912, 2913	11488, 2403, 1578
R_{int}	0.059	0.051
$(\sin q/l)_{max}$ (Å^{-1})	0.625	0.602
$R[F^2 > 2s(F^2)]$, $wR(F^2)$, S	0.057, 0.106, 1.15	0.043, 0.109, 1.00
No. of refl./par.	3912/230	2403/156
$D\tilde{n}_{max}$, $D\tilde{n}_{min}$ (e Å^{-3})	0.56, –0.34	0.23, –0.20

Table 2 Selected geometric parameters (Å, deg) for **1** and **2** together with calculated values obtained using DFT method (B3LYP/LanL2DZ).

$[VO(L)(NCS)_2]$ (**1**)	exp	calc		exp	calc
V1—O1	1.592(2)	1.59629	V1—N22	2.103(3)	2.14108
V1—N3	2.015(3)	1.97106	V1—N12	2.108(3)	2.14107
V1—N2	2.019(3)	1.97106	V1—N1	2.350(3)	2.46103
O1—V1—N3	102.14(12)	107.016	N2—V1—N12	159.75(11)	153.966
O1—V1—N2	100.98(12)	107.014	N22—V1—N12	87.07(10)	84.984
N3—V1—N2	87.73(12)	90.774	O1—V1—N1	170.56(11)	169.442
O1—V1—N22	99.60(11)	98.537	N3—V1—N1	83.60(10)	80.173
N3—V1—N22	158.25(11)	153.968	N2—V1—N1	86.62(11)	80.171
N2—V1—N22	88.72(11)	86.378	N22—V1—N1	74.77(9)	73.841
O1—V1—N12	99.25(11)	98.540	N12—V1—N1	73.16(9)	73.841
N3—V1—N12	88.88(11)	86.378			
$[VO(L)(NCS)_2]C_6H_5CH_3$ (**2**)	exp	calc		exp	calc
V1—O1	1.582(3)	1.59696	V1—N12	2.115(2)	2.13924
V1—N2	2.024(2)	1.97625	V1—N12^{i}	2.115(2)	2.13925
V1—N2^{i}	2.024(2)	1.97624	V1—N1	2.349(3)	2.42885
O1—V1—N2	102.27(9)	106.006	N12—V1—N12^{i}	84.96(11)	85.004
N2—V1—N2^{i}	89.35(12)	91.526	O1—V1—N1	171.74(12)	169.129
O1—V1—N12	99.52(9)	97.890	N2—V1—N1	83.52(8)	81.379
N2—V1—N12	88.73(8)	86.691	N12—V1—N1	74.52(7)	74.254
N2^{i}—V1—N12	158.03(9)	155.562			

Symmetry code(s): (i) *x*, –*y*+1/2, *z*.

Table 3. Selected hydrogen bonds parameters (Å, deg) for **1** and **2**.

D—H···*A*	*D*—H	H···*A*	*D*···*A*	*D*—H···*A*
$[VO(L)(NCS)_2]$ (**1**)				
N1—H1···O1^{i}	0.98	2.21	3.104 (3)	151.5
C16—H16B···O1	0.96	2.49	3.175 (4)	128.3
C16—H16B···S2^{ii}	0.96	3.01	3.608 (4)	121.4
C17—H17C···S2^{i}	0.96	3.02	3.921 (4)	158.0
C18—H18A···S2^{i}	0.97	2.87	3.820 (3)	167.5
C27—H27B···S4^{i}	0.96	2.96	3.784 (4)	144.6
$[VO(L)(NCS)_2]\cdot$Tol (**2**)				
C16—H16A···O1	0.96	2.45	3.181 (4)	133.2

Symmetry code(s): (i) –*x*+1/2, *y*–1/2, –*z*+1/2; (ii) –*x*+1/2, *y*+1/2, –*z*+1/2.

Table 4 Selected infrared bands observed in $VOL^1(NCS)_2$ (**1**) and $[VOL^1(SCN)_2]\cdot C_6H_5CH_3$ (**2**). All values in cm^{-1}.

1	**2**		
Experiment (IR)		Calculations (B3LYP/LanL2DZ)	Approximate description[b]
474 w	471wsh		
489 vw	479w 483w	467	NCS b
618w	630w	645	oop ring def. (L^D)
667	663w 675m	678	oop ring def. (L^D) + NH b
-	755w	728	oop ring def. (toluene)
807		776	CH b oop (toluene)
817	814m	788	NH b
908	907m	858	CH b oop (L^D)
		885	NCN b + NH b + CN s (amine)
973m	983m	1070	VO s
1060m	1059m		
1103m	1114m		
1245m	1246m	1184 1262	CN s asym (amine) NN s + N-CH_2 s asym
1280m	1270m	1278	NN s + N-CH_2 s sym
1389m	1387m	1414 1470	CN s (rings) + CNN b + CH_2 t CN s (rings) + CH_3 sc
1415m	1421m	1494	CN s (rings) + C-CH_3 s
1452	1460m		
1471m	1471m 1494sh	1526	Complex band (>10 normal modes) mainly sc in CH_2 and CH_3 (L^D and toluene)
1556m	1555m	1598	CC s (L^D)
2047	2062ssh	2093	CN s (NCS) asym
2070	2077s	2120	CN s (NCS) sym

[a] b=broad, vw=very weak, w=weak, m=medium, s=strong, sh=shoulder
[b] s=stretching, b=bending, w=wagging, t=twisting, r=rocking, sc=scissoring, def.=deformation, sym=symmetrical, asym=asymmetrical, oop=out-of-plane

Table 5 Assigned transitions (in cm^{-1}) on diffuse reflectance and absorbance in methanol solution spectra of $[VOL^1(SCN)_2]\cdot C_6H_5CH_3$ and extinction coefficients (ε) and crystal field (CF) parameters.

Transitions	Absorbance	ε($M^{-1}cm^{-1}$)	Reflectance
$^2B_{2g} \rightarrow {}^2E$	13550	(53)	13090
$^2B_{2g} \rightarrow {}^2B_{1g}$	17100	(26)	18335
$^2B_{2g} \rightarrow {}^2A_1$	26560	(30)	26090
CT	32260	(2890)	31150 br
CT	37590	(4710)	36050 br
Crystal field parameters (cm^{-1})			
Dq	1710		1833
Dt	738		831
Ds	-3287		-2978

Table 6 The most intensive transitions (with oscillator strength higher than 0.02) calculated for $[VOL^1(SCN)_2]\cdot C_6H_5CH_3$.

Energy (cm-1)	Osc. Strength	Major contribs	Character
25941	0.0264	H-3(A)→LUMO(A) (43%), H-2(A) →L+1(A) (37%)	L^{NCS} to VO
26178	0.0337	H-2(A) →LUMO(A) (27%), H-3(B) →LUMO(B) (50%), H-1(B) →L+1(B) (10%)	L^{NCS} to VO
30406	0.0703	H-2(B) →L+1(B) (45%), H-1(B) →L+2(B) (31%)	L^{NCS} to VO
30447	0.0205	H-2(B) →L+2(B) (15%), H-1(B) →L+1(B) (67%)	L^{NCS} to VO
31874	0.0471	H-3(B) →L+2(B) (48%), H-2(B) →L+2(B) (21%)	L^{NCS} to VO
40272	0.0273	H-8(A) →L+1(A) (10%), H-7(B) →LUMO(B) (30%), H-6(B) →LUMO(B) (13%)	L^1 to VO
41753	0.0294	H-8(B)->LUMO(B) (29%), H-3(B)->L+7(B) (13%)	L^1/L^{NCS} to VO
42213	0.0202	H-4(A) →L+2(A) (20%), HOMO(A) →L+8(A) (39%)	L^{NCS} to VO/VO to L^1
42582	0.0852	H-3(B) →L+8(B) (19%), H-1(B) →L+7(B) (12%)	L^{NCS} to VO
42647	0.0577	H-4(A) →L+2(A) (10%), H-9(B) →LUMO(B) (10%), H-2(B) →L+7(B) (15%)	L^{NCS} to VO/L^1 to VO/VO to L^1
49404	0.0311	H-3(B) →L+12(B) (17%), HOMO(B)→L+17(B) (19%)	L^{NCS} to L^{NCS}/L^1
49527	0.0454	H-7(A) →L+3(A) (15%), H-6(B) →L+3(B) (41%)	L^1 to L^1
49785	0.0275	H-7(B) →L+4(B) (28%), H-6(B) →L+4(B) (14%)	L^1 to L^1

Table 7 IC_{50} values [μM] of tested compounds at inhibiting the proliferation of tumour (Hep G2, A549, SW480, SW 620) and non-tumour (BJ and CHO-K1) cell lines, as determined by the MTT assay. Results are means ± SD (4 experiments).

Compound	HEP G2	A549	SW 480	SW 620	BJ fibroblasts	CHO-K1
$[VOL^1(SCN)_2]C_6H_5CH_3$	345,1±9,7	356,9±14,1	323,6±8,8	635,9±9,6	189,6±10,9	49,3±7,7
$VOSO_4 \cdot 5H_2O$	>700	>700	>700	>700	245,1±12,9	39,6±8,1
NH_4NCS	n.d.	n.d.	n.d.	n.d.	n.d.	n.d.

Supplementary Data (Figures S1-S2 and Tables S1).

Table S1 HOMO and LUMO energy values (in eV) calculated by DFT method

Parameters	Compound	B3LYP/LanL2DZ
E_{total} (hartree)	**1**	-1095
	2	-1367
HOMO energy (eV)	**1**	-5.42 (α-spin, SOMO)
	2	-5.55 (α-spin, SOMO)
LUMO energy (eV)	**1**	-1.77
	2	-1.88
$\Delta E_{HOMO-LUMO}$ (eV)	**1**	3.65
	2	3.67

1 hartree = 627.5095 kcal/mol = 27.2116 eV

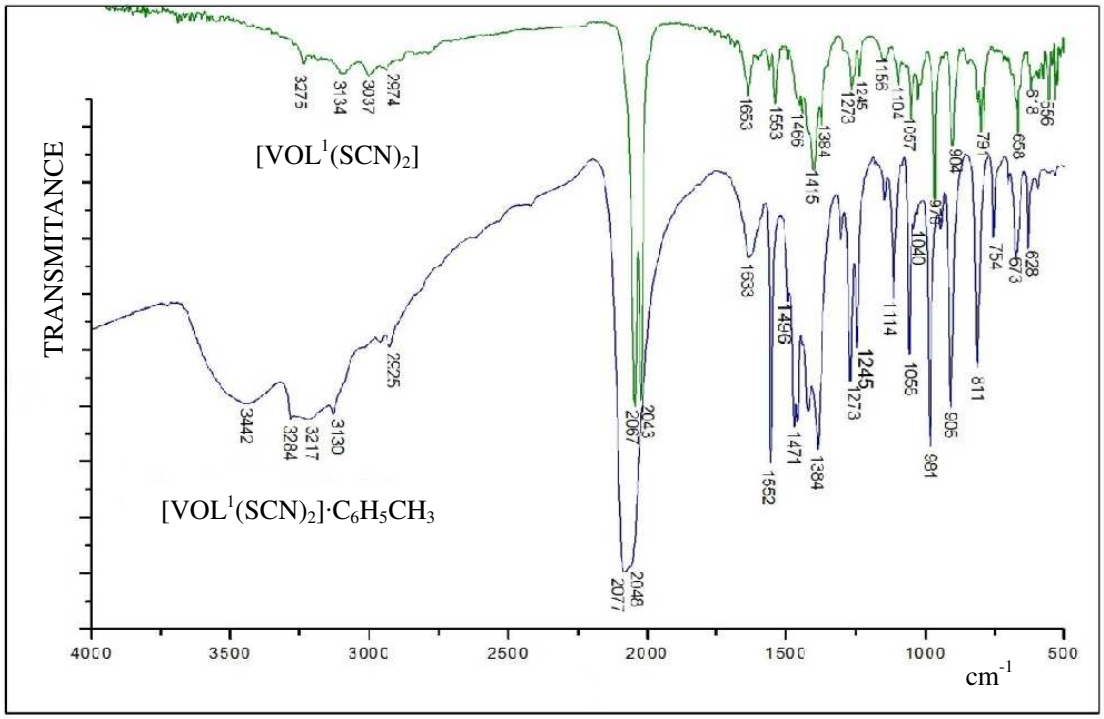

Fig S1 . Experimental infrared absorption spectra of $[VOL^1(SCN)_2]$ (**1**) and $VOL^1(SCN)_2]\cdot C_6H_5CH_3$ (**2**).

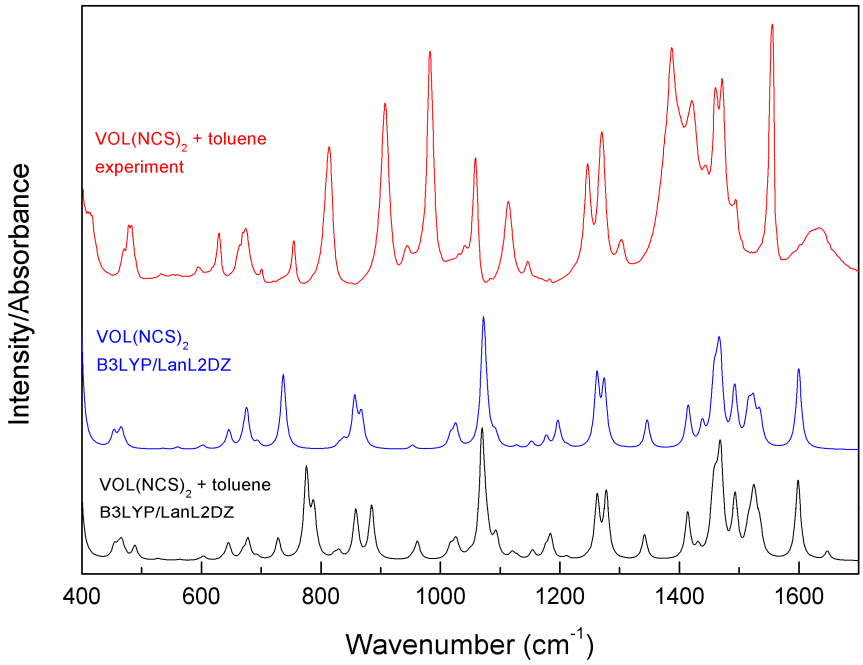

Fig. S2 The calculated infrared absorption spectra of **1** (blue) and **2** (black) together with the experimental spectrum of **2** (red). The spectra were vertically offset for clarity.

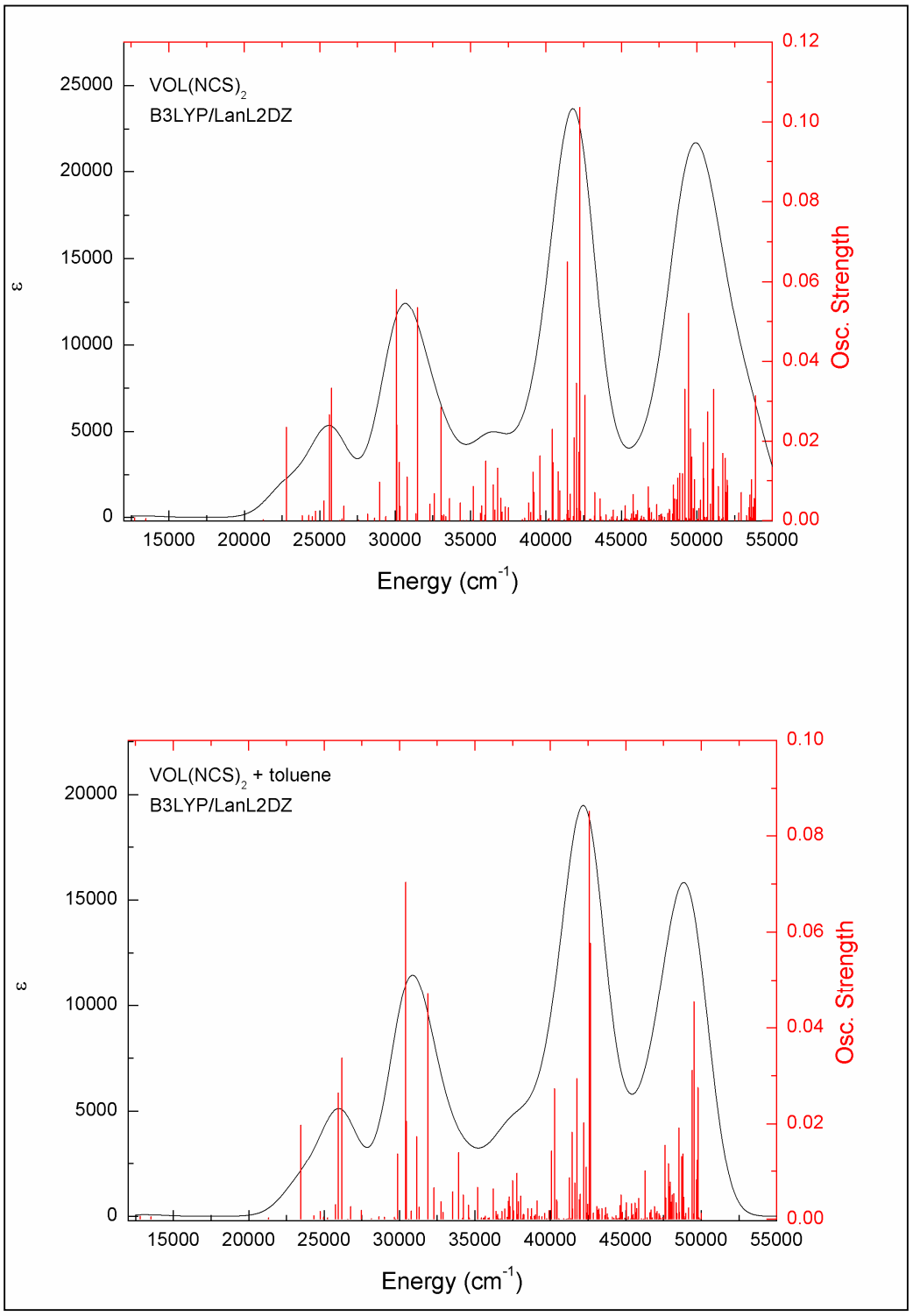

Fig. S3. Calculated transitions (red colour, right scale) with the convoluted electronic absorption spectrum (black colour, left scale) of **1** and **2**. Theory level: B3LYP/LanL2DZ.

Fig. 1.(a) Molecular structure of $[VOL^1(NCS)_2]$ (**1**) and (b) $[VOL^1(NCS)_2]\cdot$Toluene (**2**).

Fig.2. Normalized Hirshfeld surface around the $[VOL^1(NCS)_2]$ molecules (a) in **1** and (b) in **2**. Chain patterns created (c) by hydrogen bonds in **1** and (d) by C–H···p interactions In **2**.

Fig 3. Contour plots of the frontier molecular orbitals of **1** (left) and **2** (right). Theory level: B3LYP/LanL2DZ

Fig. 4. Diffuse reflectance spectra of $[VOL^1(SCN)_2]\cdot C_6H_5CH_3$ (2) and (insert) absorption spectrum of (2) in methanol ($2\cdot10^{-3}$ M, $\varepsilon/M^{-1}cm^{-1}$)

Table 1. Crystal data and structure refinement for **1** and **2**.

Table 2. Selected geometric parameters (Å, deg) for **1** and **2** together with calculated values obtained using DFT method (B3LYP/LanL2DZ).

Table 3. Selected hydrogen bonds parameters (Å, deg) for **1** and **2**.

Table 4. Selected infrared bands observed in $VOL^1(NCS)_2$. All values in cm^{-1}.

Table 5. Assigned transitions (in cm^{-1}) on diffuse reflectance and absorbance in methanol solution spectra of $[VOL^1(SCN)_2]\cdot C_6H_5CH_3$ and extinction coefficients (ε) and crystal field (CF) parameters.

Table 6. The most intensive transitions (with oscillator strength higher than 0.02) calculated for **2**.

Table 7. IC_{50} values [μM] of tested compounds at inhibiting the proliferation of tumour (Hep G2, A549, SW480, SW 620) and non-tumour (BJ and CHO-K1) cell lines, as determined by the MTT assay. Results are means ± SD (4 experiments).

Fig S1. Experimental infrared absorption spectra of $[VOL^1(SCN)_2]$ (**1**) and $[VOL^1(SCN)_2]\cdot C_6H_5CH_3$ (**2**).

Fig S2. Calculated infrared absorption spectra of **1** (blue) and **2** (black) together with experimental spectrum of **2** (red). The spectra were vertically offset for clarity.

Fig. S3. Calculated transitions (red colour, right scale) with the convoluted electronic absorption spectrum (black colour, left scale) of **1** and **2**. Theory level: B3LYP/LanL2DZ.

Table S1. HOMO and LUMO energy values (in eV) calculated by DFT method